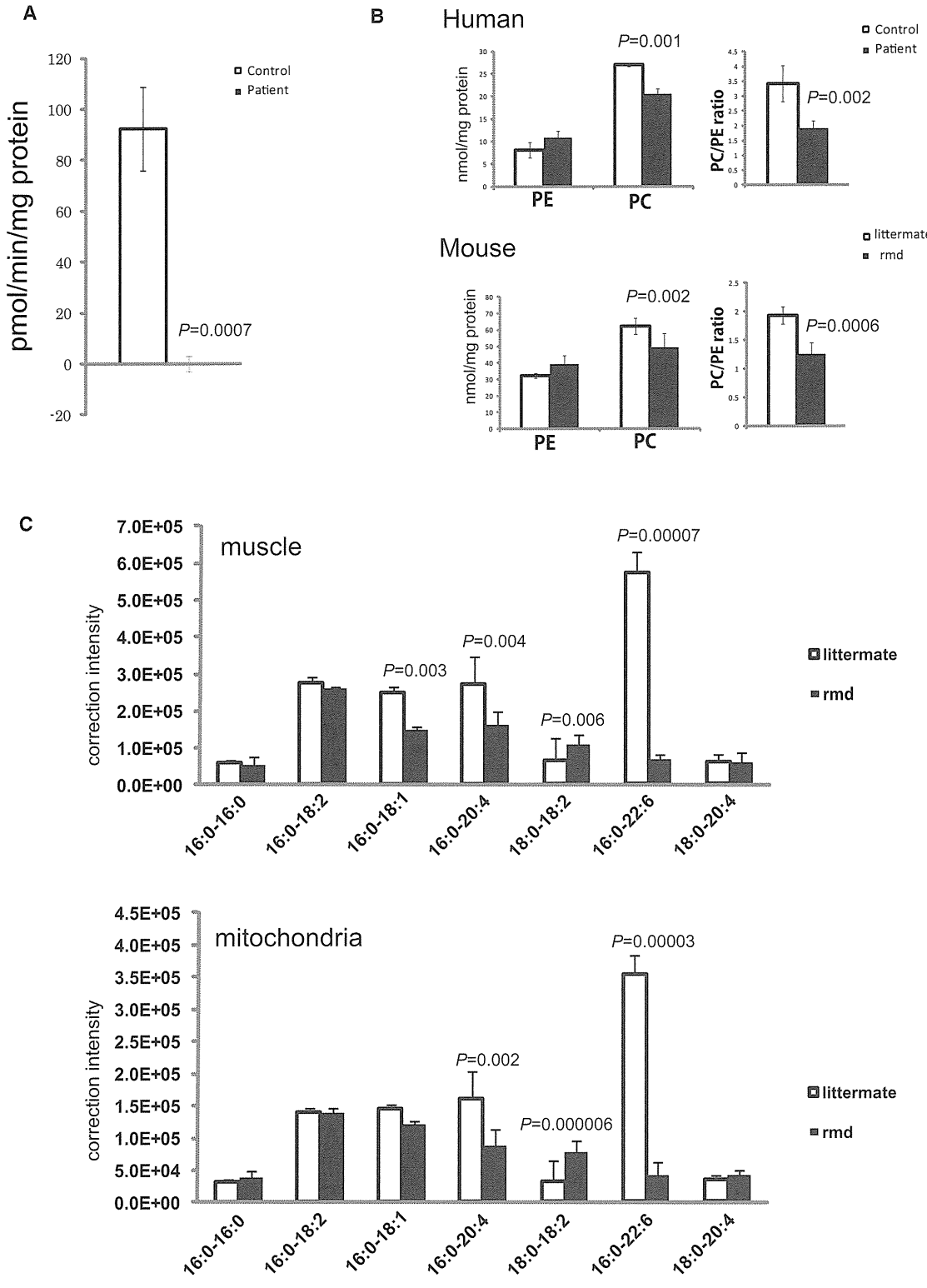

Figure 2. Choline Kinase Activity and Phospholipid Analyses
(A) In muscle tissue from individuals 2, 3, and 4, CHK activity cannot be detected (n = 3). Data represent the mean of three individuals. (B) PC and PE content in frozen biopsied muscle tissues from individuals 2, 3, and 4 and hindlimb muscles from 8-week-old *rmd* mice (n = 4) and control littermates (n = 5) were analyzed by thin-layer chromatography followed by phosphorus analysis. PC and the PC/PE ratio are significantly decreased in affected individuals and *rmd* mice (n = 3 for humans, n = 4 for *rmd* mice, n = 5 for littermates). (C) Fatty acid composition of PC molecular species in muscles and isolated mitochondria from hindlimb muscles of *rmd* mice are determined by electrospray ionization mass spectrometry (ESI-MS). We observed that 34:1-PC (16:0-18:1), 36:4-PC (16:0-20:4), and 38:6-PC (16:0-22:6) species are significantly decreased, whereas 36:2-PC (18:0-18:2) is increased in *rmd* muscle. Similarly, in isolated mitochondria from hindlimb muscle, 36:4-PC (16:0-20:4) and 38:6-PC (16:0-22:6) species are decreased, whereas 36:2-PC (18:0-18:2) is increased.

chromosomes. To elucidate the pathogenesis of these substitutions, we measured CHK activity in recombinant proteins with mutations. We cloned the open reading frame of *CHKB* into pGEM-T easy (Promega), then subcloned it into pET15b (Novagen) to make His-tagged CHK-β.[8] Each mutation was induced by site-directed mutagenesis.[7] Plasmids were transformed into *Escherichia coli* strain BL21 (DE3) and inoculated at 20°C to an OD_{600} of approximately 0.5, and the addition of 0.4 mM isopropyl-β-D-thiogalactopyranoside induced expression. The His-tagged CHK-β proteins were subjected to affinity purification on a nickel column (GE Healthcare) and eluted with 20 mM Tris-HCl (pH 7.4), 0.5 M NaCl, 300 mM imidazol, and 1 mM phenylmethanesulfonyl fluoride, and 25 ng protein was analyzed for CHK activity. CHK activity of recombinant proteins with these mutations decreased to less than 30% of wild-type CHK activity, suggesting that these mutations are causative in these individuals (Figure S2). For individual 13, who had a mutation at the splice site of the exon-intron border after exon 9 (c.1031+1G>A), we also analyzed cDNA sequences. Exons 4 through 10 were amplified from the first-strand cDNAs, and direct sequencing followed. cDNA analysis of *CHKB* in skeletal muscle from individual 13 showed four splicing variants, all of which remove consensus domains for *CHKB* (Figure S3). This suggests the same loss-of-function mechanism in humans and *rmd* mice.

Because phosphorylation of choline by CHK is the first enzymatic step for phosphatidylcholine (PC) biosynthesis,[9] we anticipated that PC content should be altered in affected individuals' muscles. Phosphatidylcholine (PC), phosphatidylethanolamine (PE), and total phospholipid amounts were measured in biopsied muscles from individuals 2, 3, and 4 and in leg muscles from 8-week-old *rmd* mice by either one-dimensional or two-dimensional thin-layer chromatography (TLC) followed by phosphorus analysis.[10,11] As expected, PC levels decreased in affected individuals' skeletal muscle (Figure 2B), as they did in *rmd* mice (Figure 2B and Sher et al.[1]), suggesting that the CMDs due to *CHKB* mutations in humans and *rmd* mice are not only pathologically but also pathomechanistically similar.

PC is present in all tissues and accounts for around 50% of phospholipids in biological membranes in eukaryotes. Selective tissue involvement can be explained by the different tissue distribution of CHK isoforms. There are two CHK isoforms: CHK-α and CHK-β, encoded by distinct genes, *CHKA* (MIM 118491) and *CHKB*, respectively. They are known to form both homodimers and heterodimers, with differential tissue distribution.[12] In mice, disruption of *Chka* causes embryonic lethality,[13] suggesting the importance of CHK-α in embryonic development. In skeletal muscles from *rmd* mice, CHK activity is absent, and PC levels are decreased.[1] In other tissues, however, CHK activity is only mildly decreased, PC levels are not altered, and no obvious pathological change is seen.[1] CHK activity in skeletal muscle from individuals 2, 3, and 4 is barely detectable, and PC levels are significantly decreased, suggesting that CHK-β is the major isoform in human skeletal muscle. In support of this notion, CHK-α was not detected in human muscle (Figure S4). These results suggest that muscular dystrophy in affected individuals and *rmd* mice is caused by a defect in muscle PC biosynthesis. In addition, in *rmd* mice, hindlimb muscles are more significantly affected than forelimb muscles.[1] This is most likely explained by the fact that CHK activity is detected, though decreased, in forelimb muscles in *rmd* mice as a result of the continued post-natal expression of *Chka*.[14] This indicates that the severity of muscle involvement is determined by the degree of deficiency of CHK activity.

Generally, phospholipids have saturated or monounsaturated fatty acids at the *sn-1* position and polyunsaturated fatty acids at the *sn-2* position of glycerol backbone.[15] It has been shown that phospholipids have tissue-specific fatty acid composition.[15] For example, heart PC and muscle PC mainly contain docosahexaenoic acid (22:6) (Nakanishi et al.[15] and Figure 2C), but liver PC includes various fatty acids.[15] NanoESI-MS analyses of PC molecular species in muscle and isolated mitochondria were performed with a 4000Q TRAP (AB SCIEX, Foster City, CA, USA) and a chip-based ionization source, TriVersa NanoMate (Advion BioSystems, Ithaca, NY, USA).[16] Quadriceps femoris (hindlimb) and Triceps (forelimb) muscle from affected *rmd* mice and littermate controls were frozen with liquid nitrogen, and total lipid was extracted by the Bligh and Dyer method.[10] The ion spray voltage was set at −1.25kV, gas pressure at 0.3 pound per square inch (psi), and flow rates at 200 nl/min. The scan range was set at m/z 400~1200, declustering potential at −100V, collision energies at −35~−45V, and resolutions at Q1 and Q3 "unit." The mobile phase composition was chloroform: methanol (1/2) containing 5 mM ammonium formate and was normalized to the muscle weight. The total lipids were directly subjected by flow injection, and selectivity was analyzed by neutral loss scanning of the polar head

In muscle and isolated mitochondria, the 38:6-PC molecular species is profoundly decreased (n = 6 for muscle, n = 5 for isolated mitochondria).

Mitochondria from skeletal muscles of whole hindlimbs of *rmd* mice were isolated by the differential centrifugation method. Fresh muscle was minced and homogenized with a motor-driven Teflon pestle homogenizer with ice-cold mitochondrial isolation buffer (10 mM Tris-HCl [pH 7.2], 320 mM sucrose, 1mM EDTA, 1mM DTT, 1 mM PMSF, 1 mg/ml BSA, and protease inhibitor cocktail [Roche]) and centrifuged at 1,500 × *g* for 5 min. The supernatant fraction was centrifuged at 15,000 × *g* for 20 min, the pellet was resuspended in mitochondrial isolation buffer, and the centrifugation/resuspension was repeated twice more.

All data are presented as means ± standard deviation (SD). Means were compared by analysis with a two-tailed t test via R software version 2.11.0.

group for PC in negative-ion mode.[17] Interestingly, there was a 10-fold decrease (9.8%) in the 16:0-22:6-PC levels versus the control in *rmd* hindlimb muscle and also in muscle mitochondria (Figure 2C), indicating the importance of the PC de novo synthesis pathway for maintaining not only PC levels but also fatty acid composition of PC molecular species. Similarly, in forelimb muscle 16:0-22:6 PC levels were also decreased in comparison to the control, but to a milder extent (18.2%), suggesting an association between severity of muscle damage and fatty acid composition alteration of PC (data not shown). In *rmd* mice, it has been shown that muscle PC can be delivered from plasma lipoprotein,[18] suggesting that non-decreased PC molecular species might be derived from the plasma, whereas 16:0-22:6 PC might be synthesized only in muscle (and possibly in brain). However, confirmation of this requires further studies.

Individuals with *CHKB* mutations have severe mental retardation in addition to the muscular dystrophy. Interestingly, polymorphisms near the *CHKB* locus and decreased CHKB expression have been associated with narcolepsy with cataplexy, suggesting a link between CHK-β activity and the maintenance of normal brain function in humans.[19] Furthermore, brain damage in pneumococcal infection has been attributed to the inhibition of de novo PC synthesis, suggesting the importance of PC synthesis for the brain.[20] Our data provide evidence that altered phospholipid biosynthesis is a causative agent for a human congenital muscular dystrophy, and further studies will elucidate the detailed molecular mechanisms of the disease in both muscle and brain.

Supplemental Data

Supplemental Data include four figures and can be found with this article online at http://www.cell.com/AJHG/.

Acknowledgments

We are grateful to the patients and their family for their participation, to Megumu Ogawa, Etsuko Keduka, Yuriko Kure, Mieko Ohnishi, Kaoru Tatezawa, and Kazu Iwasawa (National Center of Neurology and Psychiatry) for their technical assistance, to Naoki Kondou and Hiroyuki Taguchi (Kao Corporation) for their kind support on mass analysis, to Osamu Fujino and Kiyoshi Takahashi (Department of Pediatrics, Nippon Medical School) for providing patient information, and to Ken Inoue (National Center of Neurology and Psychiatry) for thoughtful comments on genetics. This study was supported partly by the Research on Psychiatric and Neurological Diseases and Mental Health of Health and Labour Sciences research grants; partly by Research on Intractable Diseases of Health and Labor Sciences research grants; partly by a Research Grant for Nervous and Mental Disorders (20B-12, 20B-13) from the Ministry of Health, Labour and Welfare; partly by an Intramural Research Grant (23-4, 23-5) for Neurological and Psychiatric Disorders from NCNP; partly by KAKENHI (20390250, 22791019); partly by Research on Publicly Essential Drugs and Medical Devices of Health and Labor Sciences research grants; partly by the Program for Promotion of Fundamental Studies in Health Sciences of the National Institute of Biomedical Innovation (NIBIO); and partly by a grant from the Japan Foundation for Neuroscience and Mental Health. G.A.C. and R.B S. were supported in part by a National Institutes of Health grant (AR-49043 to G.A.C.).

Received: March 21, 2011
Revised: April 21, 2011
Accepted: May 10, 2011
Published online: June 9, 2011

Web Resources

The URLs for data presented herein are as follows:

GenBank, http://www.ncbi.nlm.nih.gov/Genbank
Online Mendelian Inheritance in Man (OMIM), http://www.omim.org
R software version 2.11.0, http://www.r-project.org/

References

1. Sher, R.B., Aoyama, C., Huebsch, K.A., Ji, S., Kerner, J., Yang, Y., Frankel, W.N., Hoppel, C.L., Wood, P.A., Vance, D.E., and Cox, G.A. (2006). A rostrocaudal muscular dystrophy caused by a defect in choline kinase beta, the first enzyme in phosphatidylcholine biosynthesis. J. Biol. Chem. *281*, 4938–4948.
2. Nishino, I., Kobayashi, O., Goto, Y., Kurihara, M., Kumagai, K., Fujita, T., Hashimoto, K., Horai, S., and Nonaka, I. (1998). A new congenital muscular dystrophy with mitochondrial structural abnormalities. Muscle Nerve *21*, 40–47.
3. Hayashi, Y.K., Matsuda, C., Ogawa, M., Goto, K., Tominaga, K., Mitsuhashi, S., Park, Y.E., Nonaka, I., Hino-Fukuyo, N., Haginoya, K., et al. (2009). Human PTRF mutations cause secondary deficiency of caveolins resulting in muscular dystrophy with generalized lipodystrophy. J. Clin. Invest. *119*, 2623–2633.
4. Liao, H., Aoyama, C., Ishidate, K., and Teraoka, H. (2006). Deletion and alanine mutation analyses for the formation of active homo- or hetero-dimer complexes of mouse choline kinase-α and -β. Biochim. Biophys. Acta *1761*, 111–120.
5. Aoyama, C., Yamazaki, N., Terada, H., and Ishidate, K. (2000). Structure and characterization of the genes for murine choline/ethanolamine kinase isozymes alpha and beta. J. Lipid Res. *41*, 452–464.
6. Ishidate, K., and Nakazawa, Y. (1992). Choline/ethanolamine kinase from rat kidney. Methods Enzymol. *209*, 121–134.
7. Matsumoto, H., Hayashi, Y.K., Kim, D.S., Ogawa, M., Murakami, T., Noguchi, S., Nonaka, I., Nakazawa, T., Matsuo, T., Futagami, S., et al. (2005). Congenital muscular dystrophy with glycosylation defects of α-dystroglycan in Japan. Neuromuscul. Disord. *15*, 342–348.
8. Mitsuhashi, H., Futai, E., Sasagawa, N., Hayashi, Y., Nishino, I., and Ishiura, S. (2008). Csk-homologous kinase interacts with SHPS-1 and enhances neurite outgrowth of PC12 cells. J. Neurochem. *105*, 101–112.
9. Aoyama, C., Liao, H., and Ishidate, K. (2004). Structure and function of choline kinase isoforms in mammalian cells. Prog. Lipid Res. *43*, 266–281.
10. Bligh, E.G., and Dyer, W.J. (1959). A rapid method of total lipid extraction and purification. Can. J. Biochem. Physiol. *37*, 911–917.
11. Rouser, G., Fkeischer, S., and Yamamoto, A. (1970). Two dimensional then layer chromatographic separation of polar

lipids and determination of phospholipids by phosphorus analysis of spots. Lipids *5*, 494–496.
12. Aoyama, C., Ohtani, A., and Ishidate, K. (2002). Expression and characterization of the active molecular forms of choline/ethanolamine kinase-α and -β in mouse tissues, including carbon tetrachloride-induced liver. Biochem. J. *363*, 777–784.
13. Wu, G., Aoyama, C., Young, S.G., and Vance, D.E. (2008). Early embryonic lethality caused by disruption of the gene for choline kinase alpha, the first enzyme in phosphatidylcholine biosynthesis. J. Biol. Chem. *283*, 1456–1462.
14. Wu, G., Sher, R.B., Cox, G.A., and Vance, D.E. (2010). Differential expression of choline kinase isoforms in skeletal muscle explains the phenotypic variability in the rostrocaudal muscular dystrophy mouse. Biochim. Biophys. Acta *1801*, 446–454.
15. Nakanishi, H., Iida, Y., Shimizu, T., and Taguchi, R. (2010). Separation and quantification of sn-1 and sn-2 fatty acid positional isomers in phosphatidylcholine by RPLC-ESIMS/MS. J. Biochem. *147*, 245–256.
16. Ikeda, K., Mutoh, M., Teraoka, N., Nakanishi, H., Wakabayashi, K., and Taguchi, R. (2011). Increase of oxidant-related triglycerides and phosphatidylcholines in serum and small intestinal mucosa during development of intestinal polyp formation in Min mice. Cancer Sci. *102*, 79–87.
17. Taguchi, R., Houjou, T., Nakanishi, H., Yamazaki, T., Ishida, M., Imagawa, M., and Shimizu, T. (2005). Focused lipidomics by tandem mass spectrometry. J. Chromatogr. B Analyt. Technol. Biomed. Life Sci. *823*, 26–36.
18. Wu, G., Sher, R.B., Cox, G.A., and Vance, D.E. (2009). Understanding the muscular dystrophy caused by deletion of choline kinase beta in mice. Biochim. Biophys. Acta *1791*, 347–356.
19. Miyagawa, T., Kawashima, M., Nishida, N., Ohashi, J., Kimura, R., Fujimoto, A., Shimada, M., Morishita, S., Shigeta, T., Lin, L., et al. (2008). Variant between CPT1B and CHKB associated with susceptibility to narcolepsy. Nat. Genet. *40*, 1324–1328.
20. Zweigner, J., Jackowski, S., Smith, S.H., Van Der Merwe, M., Weber, J.R., and Tuomanen, E.I. (2004). Bacterial inhibition of phosphatidylcholine synthesis triggers apoptosis in the brain. J. Exp. Med. *200*, 99–106.

Human Molecular Genetics, 2011, Vol. 20, No. 19 **3841–3851**
doi:10.1093/hmg/ddr305
Advance Access published on July 12, 2011

Muscle choline kinase beta defect causes mitochondrial dysfunction and increased mitophagy

Satomi Mitsuhashi[1], Hideyuki Hatakeyama[2], Minako Karahashi[3], Tomoko Koumura[3], Ikuya Nonaka[1], Yukiko K. Hayashi[1], Satoru Noguchi[1], Roger B. Sher[4], Yasuhito Nakagawa[3], Giovanni Manfredi[5], Yu-ichi Goto[2], Gregory A. Cox[4] and Ichizo Nishino[1,*]

[1]Department of Neuromuscular Research and [2]Department of Mental Retardation and Birth Defect Research, National Institute of Neuroscience, National Center of Neurology and Psychiatry, Tokyo, Japan, [3]School of Pharmaceutical Sciences, Kitasato University, Tokyo, Japan, [4]The Jackson Laboratory, Bar Harbor, ME, USA and [5]Weil Medical College of Cornell University, New York, NY, USA

Received May 17, 2011; Revised and Accepted July 7, 2011

Choline kinase is the first step enzyme for phosphatidylcholine (PC) *de novo* biosynthesis. Loss of choline kinase activity in muscle causes rostrocaudal muscular dystrophy (*rmd*) in mouse and congenital muscular dystrophy in human, characterized by distinct mitochondrial morphological abnormalities. We performed biochemical and pathological analyses on skeletal muscle mitochondria from *rmd* mice. No mitochondria were found in the center of muscle fibers, while those located at the periphery of the fibers were significantly enlarged. Muscle mitochondria in *rmd* mice exhibited significantly decreased PC levels, impaired respiratory chain enzyme activities, decreased mitochondrial ATP synthesis, decreased coenzyme Q and increased superoxide production. Electron microscopy showed the selective autophagic elimination of mitochondria in *rmd* muscle. Molecular markers of mitophagy, including Parkin, PINK1, LC3, polyubiquitin and p62, were localized to mitochondria of *rmd* muscle. Quantitative analysis shows that the number of mitochondria in muscle fibers and mitochondrial DNA copy number were decreased. We demonstrated that the genetic defect in choline kinase in muscle results in mitochondrial dysfunction and subsequent mitochondrial loss through enhanced activation of mitophagy. These findings provide a first evidence for a pathomechanistic link between *de novo* PC biosynthesis and mitochondrial abnormality.

INTRODUCTION

Phosphatidylcholine (PC) is the major phospholipid in eukaryotic cell membranes. Disruption of PC synthesis by loss-of-function mutations in *CHKB* (GenBank Gene ID 1120), which encodes the primary choline kinase isoform in muscle, causes autosomal recessive congenital muscular dystrophy with mitochondrial structural abnormalities in human (1). Loss-of-function mutation in the murine ortholog, *Chkb,* is reported to cause rostrocaudal muscular dystrophy (*rmd*) in the laboratory mouse (2). *Rmd* is so-named because of a gradient of severity of muscle damage—hindlimbs (caudal) are affected more severely than forelimbs (rostral). The most outstanding feature of the muscle pathology in both human patients and *rmd* mice is a peculiar mitochondrial abnormality—mitochondria are greatly enlarged at the periphery of the fiber and absent from the center.

Mitochondria have a variety of cellular functions from energy production to triggering apoptotic cell death (3,4). Inhibition of mitochondrial respiration [chemically or by mitochondrial DNA (mDNA) mutations], disruption of inner membrane potential, senescence and enhanced reactive oxygen species (ROS) production are all known to cause mitochondrial morphological abnormalities (5–8). Conversely,

*To whom correspondence should be addressed at: Department of Neuromuscular Research, National Institute of Neuroscience, National Center of Neurology and Psychiatry, 4-1-1 Ogawahigashi-cho, Kodaira, Tokyo 187-8502, Japan. Tel: +81 423461712; Fax: +81 423461742; Email: nishino@ncnp.go.jp

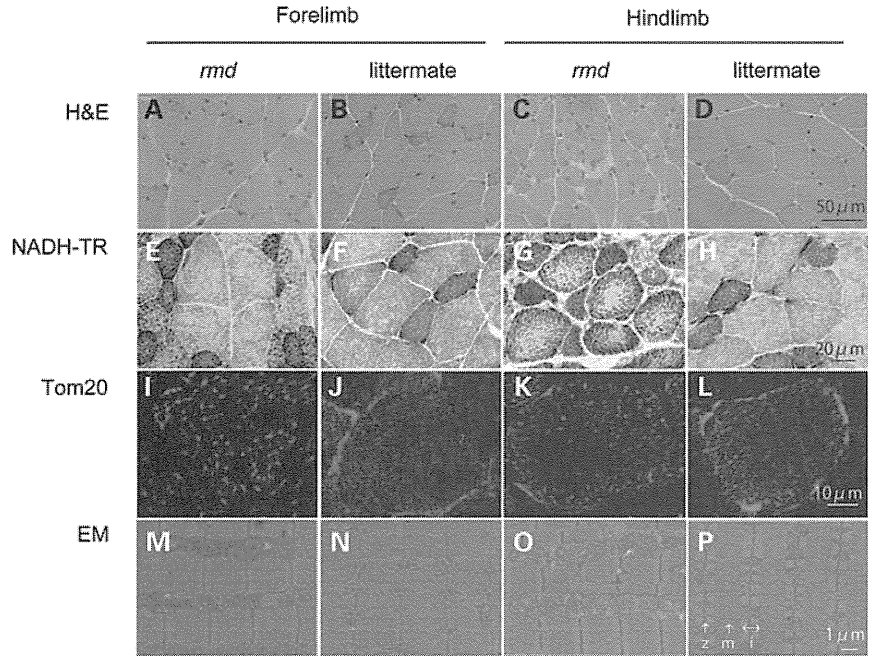

Figure 1. Muscle histopathology. H&E staining of triceps or quadriceps femoris muscles in 8-week-old homozygous *rmd* mutant mice and unaffected (+/*rmd* or +/+) littermate controls (**A**–**D**) shows dystrophic changes including variation in fiber size, necrosis and regeneration of individual fibers and interstitial fibrosis. NADH-TR staining (**E**–**H**), immunostaining of mitochondrial outer membrane protein Tom20 and EM (**M**–**P**) show abnormal mitochondria. Mitochondria in *rmd* muscle fibers are enlarged and prominent at the periphery, but sparse in the center (**I**–**L**). z, Z line; m, M line; i, I band.

primary mitochondrial morphological changes can subsequently cause mitochondrial and cellular dysfunction. Mitochondria are dynamic organelles, which continuously fuse and divide. Disequilibrium of mitochondrial fusion and fission can cause alterations of mitochondrial morphology with mitochondrial dysfunction (9,10). Thus, mitochondrial function and morphology are tightly linked.

It has been reported that mitochondria in *rmd* show decreased membrane potential (11). However, there have been no further studies about mitochondrial functional abnormalities in *rmd*, although its morphology is the most distinct feature compared with other myopathies. In addition, there has been no study about mitochondrial function when PC synthesis is blocked *in vivo*, although mitochondrial respiratory enzyme activities are dependent on membrane phospholipids (12). We hypothesized that the mitochondrial morphological abnormality in *rmd* muscle indicates the presence of a bioenergetic dysfunction caused by mitochondrial membrane phospholipid alteration.

In this study, we demonstrate that mitochondria in *rmd* mouse muscle show reduced PC level, bioenergetic dysfunction and increased ROS production are ubiquitinated and eliminated via mitophagy, leading to the peculiar mitochondrial loss in the skeletal muscle. These findings provide further evidence that mitochondrial dysfunction is related to phospholipid metabolism and may play a role in the pathogenesis of muscle disease.

RESULTS

Light microscopic examination of H&E-stained samples from 8-week-old homozygous *rmd* mutant mice and littermate controls confirmed dystrophic muscle pathology, especially in hindlimb muscles, as previously described (2) (Fig. 1A–D). NADH-TR and immunohistochemistry for mitochondrial outer membrane protein Tom20 also showed that mitochondria were sparse in the muscle fiber both in forelimb and hindlimb muscles of *rmd* mice, while the remaining mitochondria were prominent (Fig. 1E–L). More striking is the mitochondrial enlargement observed by EM (Fig. 1M–P). Mitochondria were rounder and massively enlarged compared with littermate controls. Normally, two mitochondria are present in almost all intermyofibrillar spaces and extend alongside the region between Z band and I bands. In muscles of *rmd* mice, mitochondria were larger than the size of the Z-I length itself, and often exceeded the size of a single sarcomere. In addition, mitochondria were seen only in some intermyofibrillar spaces leaving many regions devoid of mitochondria.

We hypothesized that the abnormal mitochondrial morphology in *rmd* skeletal muscles reflects altered PC content in mitochondrial membranes, as these mitochondria lack the PC biosynthetic pathway. We therefore measured PC, PE and CL in isolated mitochondria (Fig. 2). PE is the second most abundant phospholipid in mitochondria and CL is a mitochondria-specific phospholipid. PC was significantly decreased to 72% in forelimb and to 61% in hindlimb muscles compared with healthy littermates, while PE levels were unchanged. The PC/PE ratio was decreased, reflecting the PC reduction. This reduction is well correlated with the phospholipid compositional alteration in muscle tissue as previously described (1,2). CL showed only a slight decrease and only in the more severely affected hindlimb muscles.

We speculated that mitochondrial function in *rmd* is altered, and therefore measured respiratory enzyme activity and ATP

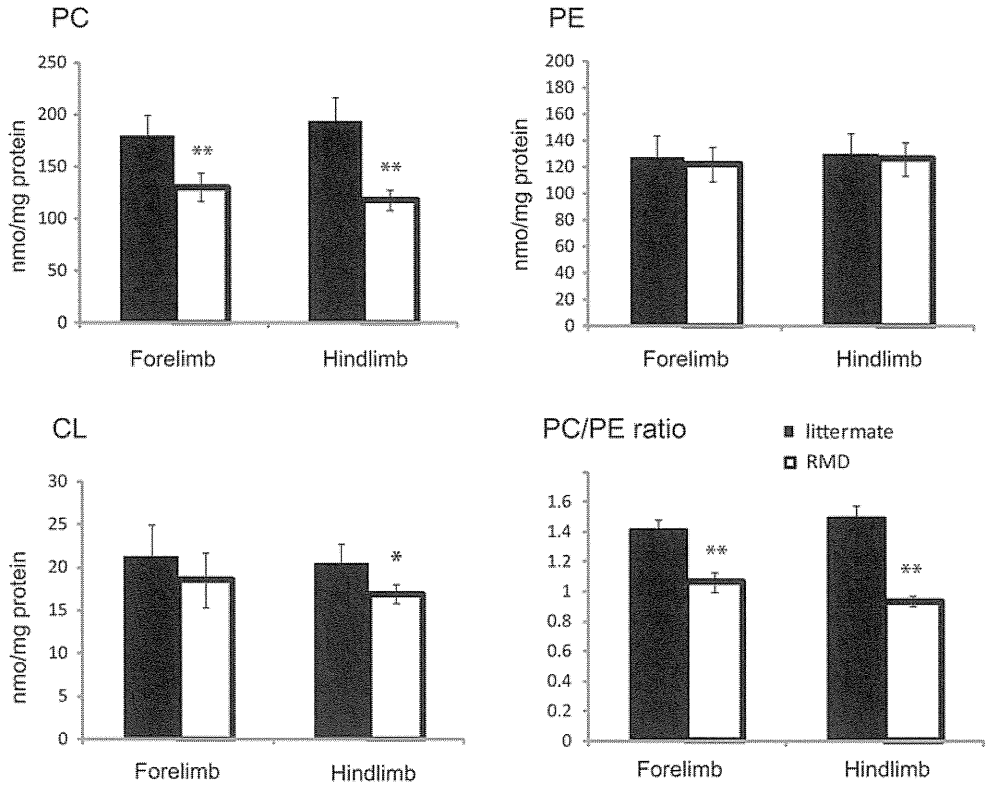

Figure 2. The PC level is decreased in *rmd* muscle mitochondria. The PE level is not altered. The PC/PE ratio is significantly decreased in *rmd*. The CL level is slightly decreased in *rmd* hindlimb. Data are expressed as the mean ± SD of eight experiments. $^{*}P < 0.01$, $^{**}P < 0.0001$.

synthesis in isolated mitochondria in *rmd* muscle. Compared with healthy littermates, only mitochondrial respiratory Complex III activity was significantly decreased in mitochondria from *rmd* forelimb muscles, while Complex I, III and IV activities were significantly decreased in *rmd* hindlimb muscles (Fig. 3A). Mitochondrial ATP synthesis was severely decreased, especially in hindlimb muscles (Fig. 3B), and coenzyme Q9 was moderately decreased in *rmd* compared with littermates (Fig. 3C).

In-gel activity staining on native PAGE showed decreased Complex III activity, especially in hindlimb (Fig. 4A), although normal protein levels of the Complex III were detected by western blot followed by Native PAGE (Fig. 4B). There was no difference in mobility of Complex III in *rmd* and littermate. Furthermore, respiratory chain supercomplex formation, which is important for effective electron transport (24), was not altered in *rmd* (Supplementary Material, Fig. S1).

Mitochondria are a major site of ROS production under normal circumstances and the production of ROS is enhanced when respiration is blocked. To determine whether the identified respiratory defects lead to elevated ROS, we measured superoxide levels from isolated mitochondria. Superoxide production was significantly increased in *rmd* muscle mitochondria, especially in those isolated from the hindlimbs (Fig. 5A). Moreover, the MDA level (Fig. 5B) and 4-hydroxynonenal adducts (Fig. 5C) were increased in *rmd* muscles indicating that oxidative stress is increased in *rmd* muscle.

Interestingly, examination of muscle sections by EM revealed autophagosomes selectively engulfing an entire mitochondrion, without cytoplasm, suggesting that mitophagy is activated in *rmd* skeletal muscles (Fig. 6A). Western blots of isolated mitochondria from muscle showed significantly increased levels of the autophagosome marker LC3 in *rmd* (Fig. 6B). In addition, polyubiquitinated proteins and p62/SQSTM1, which connects ubiquitination and autophagic machineries, were also increased in isolated mitochondria (Fig. 6B). These data suggest that mitochondria are polyubiquitinated and p62 is recruited to mitochondria. We also analyzed PINK1 and the E3 ubiquitin ligase Parkin, which are known to contribute to ubiquitination and mitophagy of damaged mitochondria (25,26). PINK1 and Parkin levels were increased in *rmd* isolated muscle mitochondria (Fig. 6B), suggesting that they were recruited to mitochondria to promote mitophagy. Immunohistochemical analyses demonstrated the colocalization of p62, polyubiquitin and LC3 with mitochondria (Fig. 6C).

We quantified mitochondrial numbers in muscle fibers, mitochondria occupying-area relative to muscle cross-sectional area and mean mitochondrial area in cross-section by morphometric analysis in EM. In *rmd*, the average number of mitochondria per fiber was profoundly decreased (Fig. 7A). However, the average area occupied by mitochondria in each muscle fiber was comparable with littermates (Fig. 7A). This was due to increased mean mitochondrial area in *rmd* (Fig. 7A).

We quantified mtDNA copy number relative to nuclear DNA. In *rmd*, mtDNA was decreased both in forelimb and

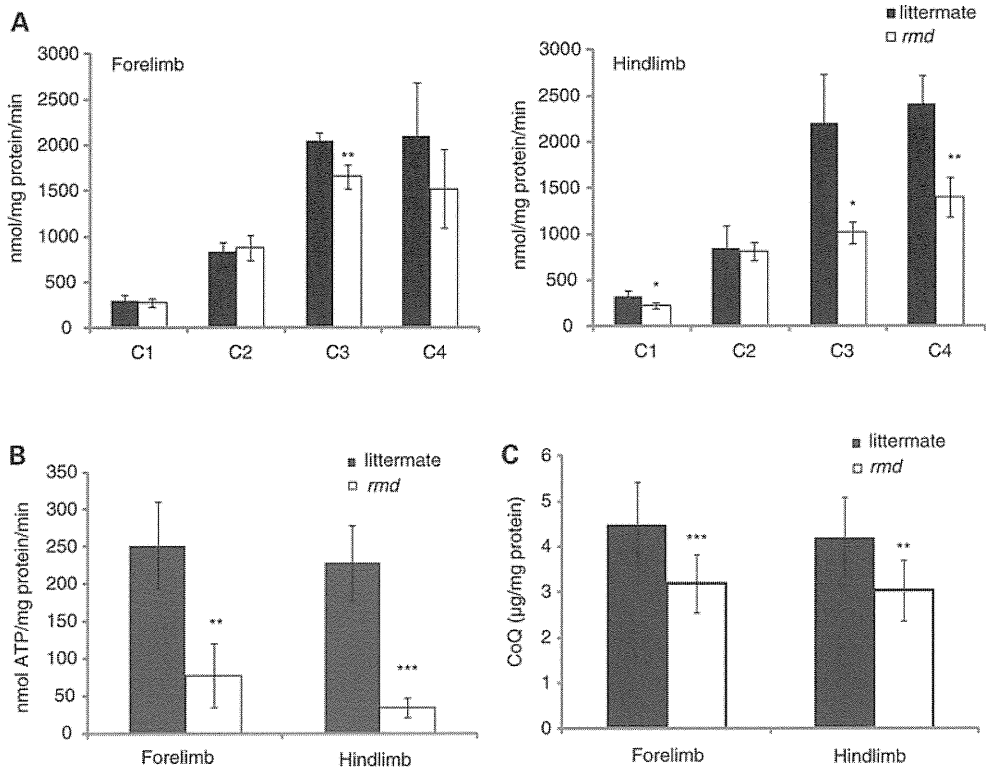

Figure 3. Mitochondrial energetic function is altered and CoQ level is decreased in *rmd*. (**A**) Mitochondrial respiratory chain enzyme activities in *rmd* were compared with healthy littermates. C1, Complex I ; C2, Complex II ; C3, Complex III ; C4, Complex IV ($n = 4$). (**B**) The rate of ATP synthesis measured by luminometry method ($n = 4$). (**C**) Total CoQ9 level (littermate forelimb, $n = 13$; littermate hindlimb, $n = 12$; *rmd* forelimb, $n = 11$; *rmd* hindlimb, $n = 13$). Data are expressed as the mean ± SD of experiment number shown as n. $^{*}P < 0.05$, $^{**}P < 0.005$, $^{***}P < 0.001$.

hindlimb muscles compared with littermate controls (Fig. 7B), which was in agreement with the number of mitochondria decrease. The mtDNA copy number in liver is preserved in *rmd*, and reduction in muscle is progressive in age.

DISCUSSION

In the *rmd* mouse, we observed greater superoxide production and more significant Complex III and ATP synthesis deficiencies in hindlimb than in forelimb muscles, correlating with the more severe caudal phenotype. PC was decreased in isolated *rmd* muscle mitochondria as a consequence of disruption of muscle PC biosynthesis because PC cannot be synthesized in mitochondria. This suggests that muscle damage in the *rmd* mouse is primarily due to mitochondrial dysfunction possibly caused by the impaired PC biosynthesis.

Why then are mitochondrial functions altered when PC is decreased? Mitochondria produce energy mainly via oxidative phosphorylation, which transfers electrons by a series of redox reactions through four enzyme complexes, and pumps protons across the mitochondrial inner membrane, producing an electrochemical proton gradient that enables ATP synthesis (3). Here, we demonstrate for the first time a Complex III activity decrease without the loss of the enzyme protein complex in *rmd* muscle mitochondria, suggesting a link between decreased PC content and Complex III activity. One possible explanation is that mitochondrial PC alterations may directly impair Complex III function by affecting lipid–protein interactions (27). PC is a component of the yeast respiratory enzyme complex, as revealed by X-ray crystallography, and thus may regulate enzyme function (28). Alteration of fatty acid composition in PC has been shown to change enzymatic activity in Complexes I, III and IV in a mouse model (29). In this model, Complex III activity is profoundly increased when n-3 fatty acid is increased. In *rmd*, it is reported that docosahexiaenoic acid containing PC, the major n-3 fatty acid in muscle PC, is profoundly decreased in muscle and in isolated mitochondria (1). This suggests a possible association between phospholipid composition alterations and respiratory chain enzymatic activities due to the choline kinase defect in *rmd* muscle.

Through the oxidative phosphorylation process, ROS are also generated as byproducts even in normal cellular states, but especially when respiration is inhibited (30,31). In *rmd* mouse muscle, ROS production from isolated mitochondria was increased, which may be related to the respiratory chain defect caused by PC reduction in mitochondria. Interestingly, selenium-deficient myopathy is associated with muscle pathology showing similar enlarged and sparse mitochondrial morphological abnormalities to the *rmd* mice and the human congenital muscular dystrophy caused by *CHKB* mutations (32). As selenium is a cofactor of glutathione peroxidase, selenium deficiency is thought to cause oxidative stress (33,34). Morphological similarity between choline kinase beta deficiency and selenium deficiency suggests that ROS may play a key role in the formation of the mitochondrial

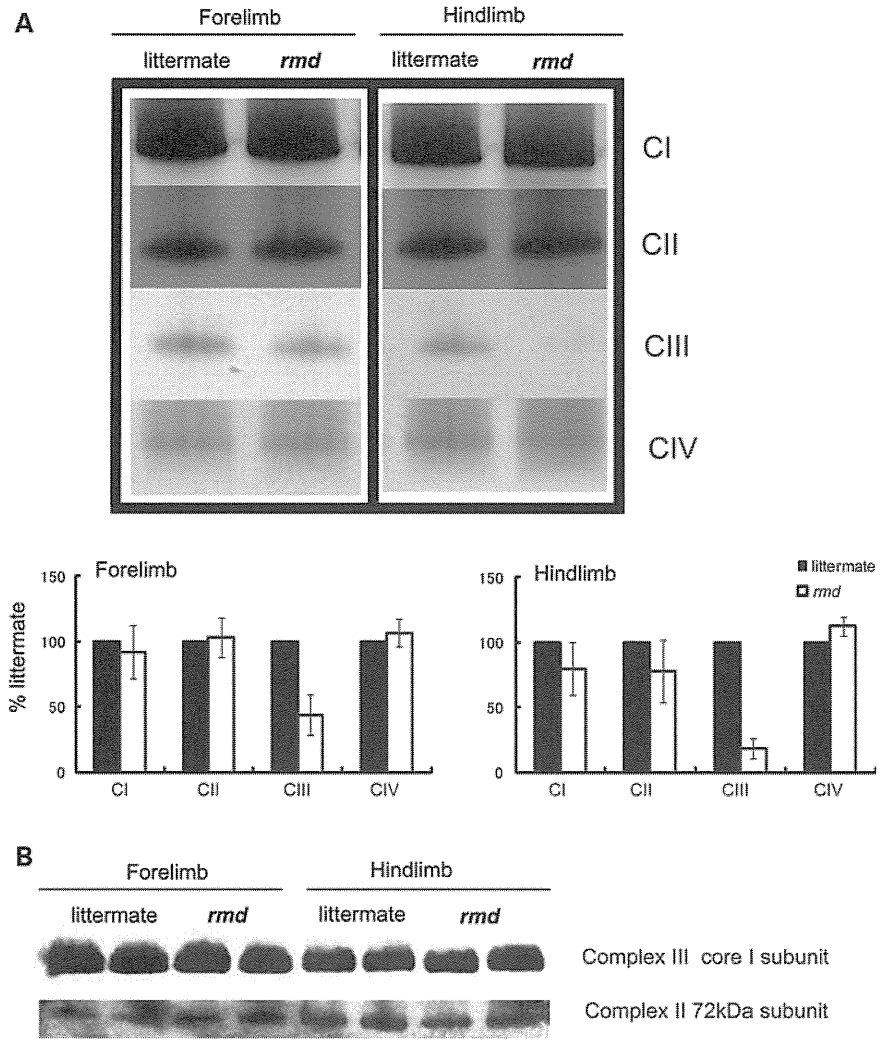

Figure 4. Mitochondrial respiratory enzyme activity is decreased without the loss of the enzyme complex. (**A**) Native PAGE gel electrophoresis. In-gel activity staining shows that Complex III activity is decreased in *rmd*. Representative data from four different experiments are shown. (**B**) Immunoblotting of Complex II and III shows protein levels are maintained despite defect in significant Complex III enzymatic activity. Representative data from three different experiments of six samples are shown.

abnormalities in *rmd* myopathy. In another model, depletion of glutathione, which provides cells with a reducing environment and detoxifies the ROS, is reported to cause mitochondria enlargement in muscle, also suggesting the possible link between mitochondrial enlargement and ROS in skeletal muscle (35).

In addition, as a major site of ROS production, mitochondria themselves are prone to ROS damage (36). Recent studies have shown that damaged mitochondria are eliminated by selective autophagy, called mitophagy, most likely as a quality control mechanism to protect the cells (37,38). In addition to mitochondrial enlargement, we observed large areas devoid of mitochondria. Mitochondrial depolarization can trigger mitophagy in cell culture models (26). PINK1 and Parkin interactions promote ubiquitination of mitochondrial outer membrane proteins, and induce mitophagy. This process is mediated by p62, an adaptor molecule, which interacts directly with ubiquitin and LC3 (25,39). ROS generated from mitochondria are also important for mitophagy (39). Interestingly, we found increased mitophagy in *rmd*, accompanied by mitochondrial ubiquitination and recruitment of p62 and LC3. Enhanced PINK1 and Parkin expression in mitochondria likely reflects the process of elimination of damaged mitochondria as a consequence of mitochondrial dysfunction and ROS production. These findings were similar to those in cells treated with the protonophore carbonyl cyanide m-chlorophenyl hydrazone (CCCP) or respiratory chain inhibitors (25,26). In *rmd*, decreased membrane potential (11), as a consequence of respiratory chain insufficiency and ROS production, may trigger mitophagy and thus increased mitochondrial clearance, which may lead to energy crisis and result in cell death and muscular dystrophy.

We observed progressive loss of mtDNA with age, together with progressive loss of mitochondria. We suggest that mtDNA depletion in this case results from increased mitophagy, because mtDNA is known to be degraded by mitophagy in cultured hepatocytes (40) and because the pathological features of CHKB-deficient myopathy are clearly distinct from those

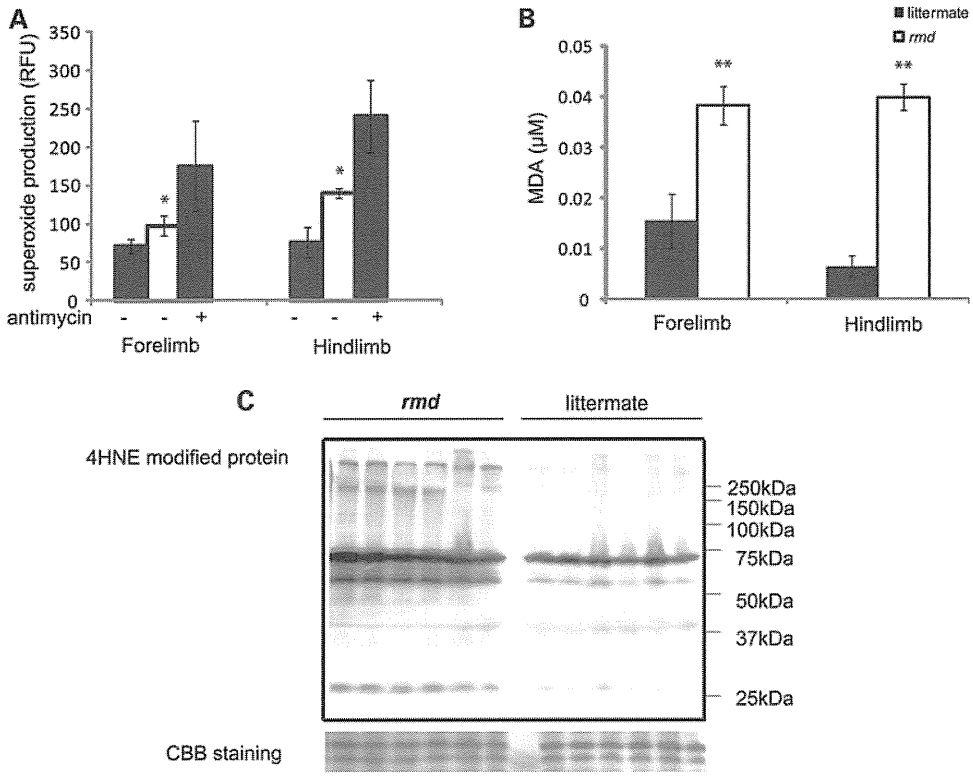

Figure 5. Mitochondrial superoxide production is increased and oxidative stress is increased in muscle tissue in *rmd*. (**A**) Mitochondrial superoxide production is enhanced in *rmd*, especially in hindlimb muscle mitochondria. Data are shown as the mean ± SD of seven experiments. $^{*}P < 0.001$. (**B**) MDA levels are increased in muscle tissue. $^{**}P < 0.0005$. Data are shown as the mean ± SD ($n = 4$ for *rmd* and $n = 5$ for littermate controls). (**C**) HNE4-modified proteins are increased in *rmd* hindlimb muscle. Coomassie brilliant blue staining is shown as a loading control. Representative data of six samples.

observed in 'primary' mtDNA depletion syndromes, usually associated with defective mtDNA synthesis, in which muscle fiber mitochondria are increased both in number and size, causing the 'ragged-red fiber' appearance (41).

In summary, we have demonstrated for the first time a pathogenic mechanism that links PC reduction in the mitochondrial membranes of *rmd* muscle to mitochondrial morphological and functional abnormalities and the induction of mitophagy as a response to structural and functional damage by ROS generation or impaired bioenergetics. These findings indicate the importance of PC *de novo* synthesis pathway and phospholipid composition of mitochondrial membrane in the maintenance of mitochondria and muscle.

MATERIALS AND METHODS

Rmd mice

Eight-week-old *rmd* mice (2) were used for all analysis and were compared with healthy littermates. The Ethical Review Committee on the Care and Use of Rodents in the National Institute of Neuroscience, National Center of Neurology and Psychiatry approved all mouse experiments.

Histological analyses

The quadriceps femoris muscles were freeze-fixed in liquid-nitrogen-cooled isopentane and stored at −80°C. Serial transverse sections of 10 μm thickness were stained with a series of histochemical methods, including hematoxylin and eosin (H&E) and nicotine amide adenine dinucleotide-tetrazolium reductase (NADH-TR), as previously described (13), and were observed by light microscopy.

Immunohistochemical analyses were performed as previously described (13). Briefly, 6 μm thick frozen muscle sections were fixed in cold acetone for 5 min. After blocking with 5% normal goat serum, sections were incubated with primary antibodies for 2 h at 37°C. After rinses with phosphate-buffered saline, sections were incubated with secondary Alexa Fluor 488- or Alexa Fluor 568-labeled goat anti-mouse

Figure 6. Mitochondrial degeneration in *rmd*. (**A**) EM of extensor digitorum longus muscle. In *rmd*, mitochondria are degraded by mitophagy. Scale bar = 0.5 μm. (**B**) Western blot of isolated muscle mitochondria immunodetected for Parkin, polyubiquitin, p62/SQSTM1 and LC3. TOM20, a mitochondrial outer membrane protein is used as loading control. Hindlimb mitochondria in *rmd* show significantly increased expression level in these mitophagy markers. (**C**) p62 and TOM20 immunohistrochemistry of hindlimb muscle section. Note that mitochondria are significantly enlarged and sparse in *rmd*. p62 colocalizes with the mitochondrial outer membrane protein TOM20. Polyubiquitin and mitochondrial protein cytochrome c oxidase (COX) colocalize. LC3 and TOM20 colocalize. Polyubiquitin and p62 colocalize. Scale bar = 10 μm.

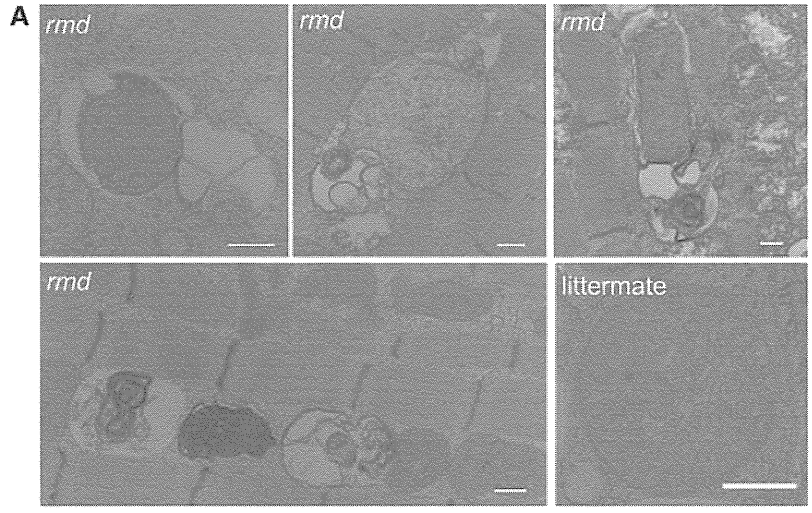

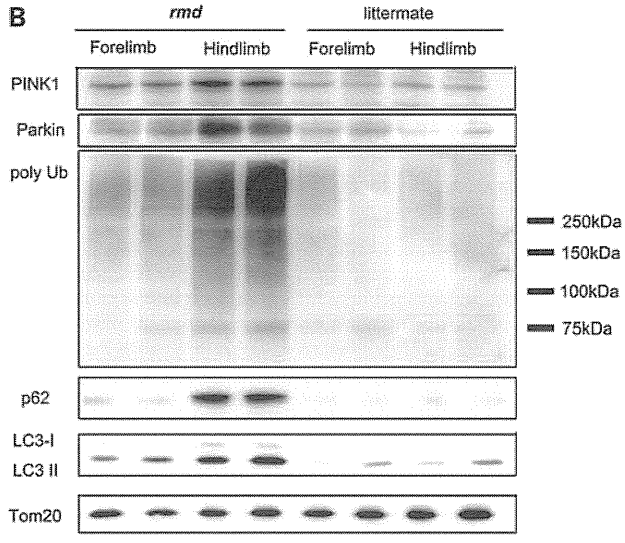

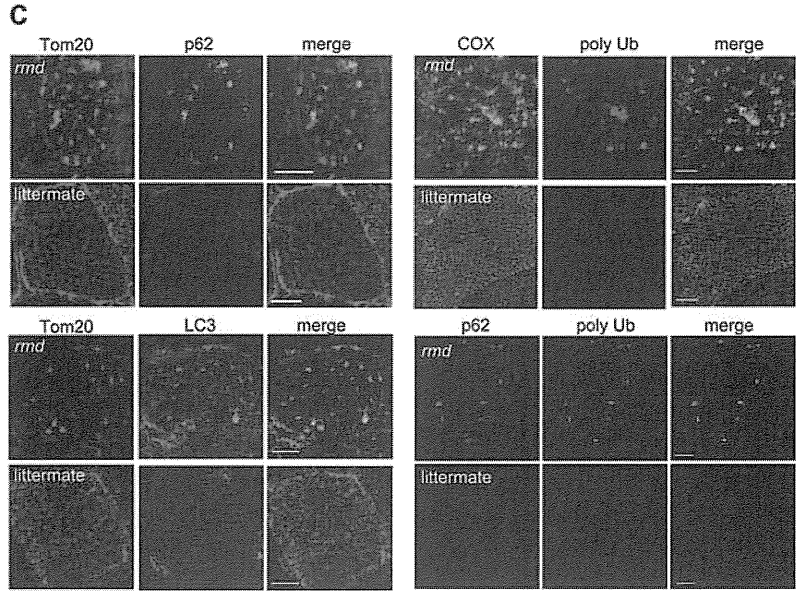

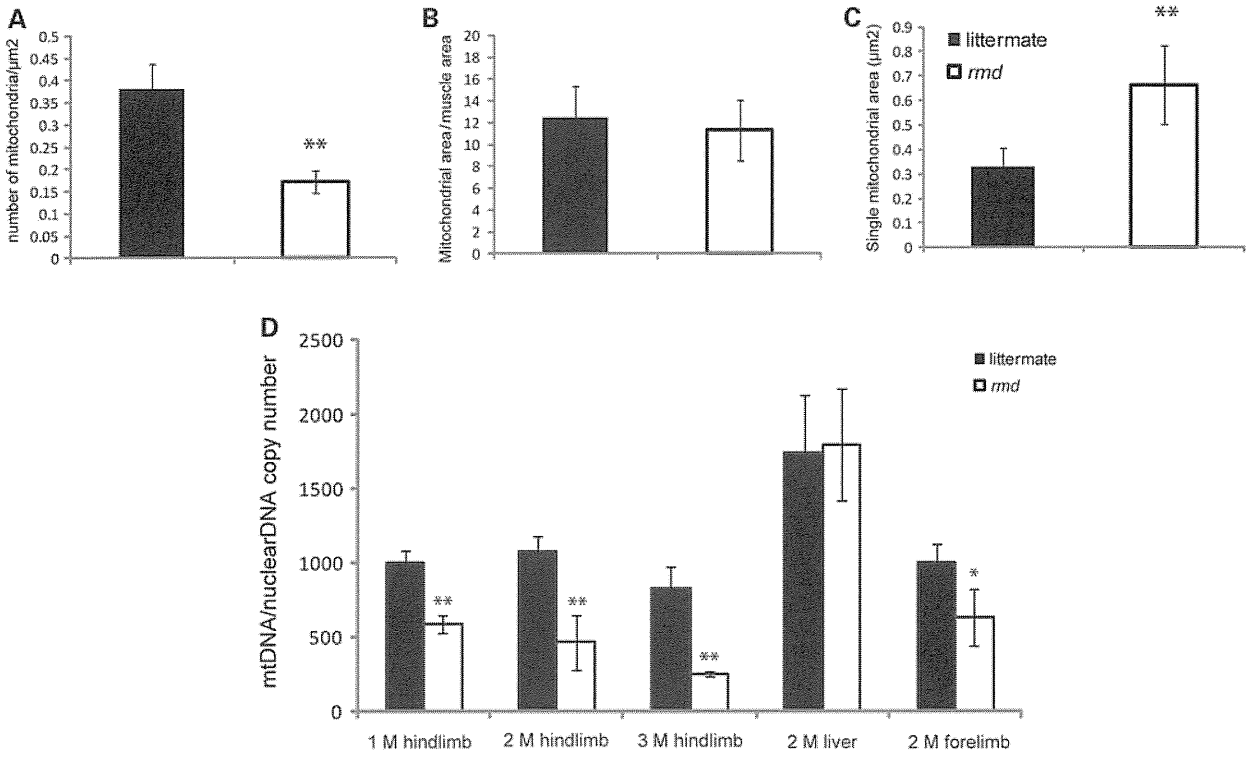

Figure 7. (**A**) Mitochondrial morphometrical analysis. All mitochondria are counted in cross-sections of EDL muscle by EM. Number of mitochondria per 1 μm^2 of muscle fiber cross-sectional area is shown ($n = 20$). The percentage of area occupied by mitochondria in a cross-section of muscle fiber is not different in *rmd* and littermates ($n = 20$). The average total mitochondrial area per muscle fiber is larger in *rmd* compared with littermates ($n = 20$). $^{*}P < 0.005$, $^{**}P < 0.0005$. (**B**) mtDNA copy number is decreased in *rmd* compared with littermate controls. Copy number of mtDNA (ND1) was normalized by nuclear DNA (*pcam1*) (M; month-old, 1 M hindlimb: *rmd*; $n = 4$, littermates; $n = 4$. 2 M hindlimb: *rmd*; $n = 5$, littermates; $n = 6$, 3 M hindlimb: *rmd*; $n = 4$, littermates; $n = 6$. 2 M liver: *rmd*; $n = 5$, littermates; $n = 5$. 2 M forelimb: *rmd*; $n = 6$, littermates; $n = 6$).

or rabbit antibodies at room temperature for 45 min. Confocal images were obtained with FLUOVIEW FV500 systems (Olympus) using a $\times 100$ objective.

For observation by electron microscopy (EM), muscle samples were fixed in 2.5% glutaraldehyde in 0.1 M cacodylate buffer. Specimens were post-fixed in 1% osmium tetroxide in the same buffer, dehydrated with graded series of ethanol and embedded in epon, as previously described (13). Ultrathin sections were stained with uranyl acetate and lead citrated, and were analyzed by a FEI Tecnai Spirit at 120 kV.

Isolation of skeletal muscle mitochondria

Mitochondria from skeletal muscle of whole forelimb and hindlimbs were isolated by differential centrifugation. Fresh muscle was minced and homogenized using a motor-driven Teflon pestle homogenizer with ice-cold mitochondrial isolation buffer [10 mM Tris–HCl pH 7.2, 320 mM sucrose, 1 mM ethylenediaminetetraacetic acid, 1 mM dithiothreitol, 1 mg/ml bovine serum albumin (BSA)] and centrifuged at 1500*g* for 5 min. Supernatant fraction was centrifuged at 15 000*g* for 20 min, and the pellet was resuspended in mitochondrial isolation buffer. The centrifugation was repeated twice. Protein concentration was determined by the Bradford method using Bio-Rad Protein Assay (Bio-Rad Laboratories), according to the manufacturer's protocol.

Lipid extraction, phospholipid separation and determination

PC, phosphatidylethanolamine (PE) and cardiolipin (CL) were extracted from isolated mitochondria of forelimb and hindlimb muscles, separated by one-dimensional thin layer chromatography (TLC) and amount of each phospholipid was measured by phosphorus analysis (14,15). Briefly, total lipids in frozen muscle biopsy samples were extracted according to the method of Bligh and Dyer (14). Each extract was evaporated to dryness under nitrogen, and the residues were then dissolved in a small amount of a 2:1 v/v mixture of chloroform and methanol and applied to a TLC plate (Merck, Silica Gel 60). The plate was developed with a medium of chloroform:-methanol:formic acid:acetic acid = 100:100:9:9 (v/v/v/v). The products and standards were visualized with primulin reagent, and the products identified by comparison with chromatographic standards. PC and PE were then scraped from the TLC plate for quantification. Phospholipids were quantified according to the method of Rouser *et al.* (15). Briefly, the lipids were digested by heating for 1 h at 200°C with 70% perchloric acid. After cooling, ammonium molybdate and ascorbic acid solution were added in that order. Color was developed after heating for 5 min in a boiling water bath. Absorbance was determined at 820 nm by spectrophotometer. Phospholipid levels were corrected by the total protein amount in isolated mitochondria.

Respiratory enzyme activity and ATP synthesis

Mitochondrial respiratory enzyme activities were measured as previously described, using colorimetric assays in isolated mitochondria (16,17). Complex I (NADH-ubiquinone oxidoreductase) activity was measured by the reduction of 10 μM decylubiquinone (DB) in the presence of 2 mM potassium cyanide (KCN), 50 μg/ml antimycin and 50 μM NADH at 272 nm. Complex II (succinate-ubiquinone oxidoreductase) activity was measured by the reduction of 50 μM 2,6-dichlorophenolindophenol in the presence of 20 mM succinate, 2.5 μg/ml rotenone, 2.5 μg/ml antimycin, 2 mM KCN and 50 μM DB at 600 nm. Complex III (ubiquinol-ferricytochrome c oxidoreductase) activity was measured by the reduction of 50 μM cytochrome c at 550 nm in the presence of 50 μM reduced DB and 2 mM KCN. Complex IV (ferrocytochrome c-oxigen oxidoreductase) activity was measured by the oxidation of 2.5 μM reduced cytochrome c at 550 nm. The activity was calculated using an extinction coefficient of 8 mM^{-1} cm^{-1}, 19.1 mM^{-1} cm^{-1}, 19.0 mM^{-1} cm^{-1} and 19.0 mM^{-1} cm^{-1} for Complexes I, II, III and IV, respectively. The specific activity of the enzymes was expressed as nmol of each substrate oxidized or reduced/min/mg of mitochondrial protein.

Mitochondrial ATP synthesis was measured by the method of Manfredi and colleagues (18). Briefly, isolated mitochondria were resuspended in 0.25 M sucrose, 50 mM 4-(2-hydroxyethyl)-1-piperazineethanesulfonic acid (HEPES), 2 mM $MgCl_2$, 1 mM ethylene glycol tetraacetic acid (EGTA) and 10 mM KH_2PO_4, pH 7.4. Then 0.15 mM P1,P5-di(adenosine) pentaphosphate, 1 mM malate, 1 mM pyruvate, luciferin and luciferase and 0.1 mM adenosine diphosphate (ADP) were added, and light emission was recorded by luminometer. For each sample, 1 mM oligomycin-added sample was used to obtain the baseline luminescence corresponding to non-mitochondrial ATP production.

CoQ9 determination

Total CoQ9 contents in isolated mitochondria were analyzed with high performance liquid chromatography (HPLC) by electrochemical detection according to the standard procedure described by Tang *et al.* (19). Briefly, isolated muscle mitochondria pellet were lysed with 2-propanol, vortexed for 1 min and centrifuged at 2000*g* for 10 min and then clear supernatant was applied for HPLC Coul Array Detector Model 5600A (ESA BIOSCIENCES, Inc.) with Capcell Pak C18 MG 100 column (3.2 I.D × 150 mm length; ESA BIOSCIENCES, Inc.). The mobile phase was degassed methanol containing 0.4% sodium acetate, 1.5% acetic acid, 1% 2-propanol and 8% n-hexane. Chromatographic data were analyzed with CoulArray Data Station 3.00 (ESA Biosciences). Standard curves were created with both oxidized and reduced CoQ9. Total CoQ9 level was determined according to the standard curve and corrected by the total protein level in isolated mitochondria as measured by the Bradford method.

High-resolution clear native PAGE

High-resolution clear native polyacrylamide gel electrophoresis (PAGE) was performed by the method of Wittig *et al.* (20). Briefly, isolated mitochondria were solubilized with Native PAGE Sample buffer (Invitrogen) containing 0.3% n--dodecyl-β-D-maltoside (Dojindo). Twenty micrograms of protein were applied to 3–12% NativePAGE Bis–Tris gel (Invitrogen). Native PAGE buffer (Invitrogen) was used for anode buffer and Native PAGE buffer containing 0.02% n--dodecyl-β-D-maltoside and 0.05% deoxycolate was used for cathode buffer.

For in-gel catalytic activity assays, gels were incubated in the following solutions: Complex I, 5 mM Tris–HCl pH 7.4, 140 μM NADH and 3 mM nitro tetrazolium blue (NTB); Complex II, 5 mM Tris–HCl pH 7.4, 20 mM succinate, 3 mM NTB and 200 μM phenazine methosulfate; Complex III, 50 mM sodium phosphate buffer pH 7.2 and 0.5 mg/ml diaminobenzidine (DAB); Complex IV, 50 mM sodium phosphate buffer (pH 7.2), 0.5 mg/ml DAB and 5 mM cytochrome c.

For immunoblotting, gels were incubated for 20 min in 300 mM Tris, 100 mM acetic acid, 1% sodium dodecyl sulfate (SDS), pH 8.6 and then electroblotted to polyvinylidene fluoride (PVDF) membrane (Millipore). Complexes II and III were detected with monoclonal antibodies against the 70 kDa subunit (Abcam) and core 2 subunit (Invitrogen), respectively.

Measurement of mitochondrial superoxide (O_2^-) production

Mitochondrial superoxide production was measured by dehydroethidium (DHE) (Molecular Probes), as described previously (21). Isolated mitochondria were incubated with 200 mM mannitol, 70 mM sucrose, 2 mM HEPES pH 7.4, 0.5 mM EGTA and 0.1% BSA. Reagents were added in the following order: 1 mM glutamate, 1 mM malate, 1 μM DHE, 0.25 mM ADP and 5 mM KH_2PO_4. Fluoresence was measured by Cytofluor 4000 (Applied biosystems) at excitation/emission = 530/620 nm.

Measurement of malondialdehyde in muscle

Malondialdehyde (MDA) levels were measured in muscle homogenates using an LPO-485 assay kit (BIOXYTEC), according to the manufacturer's protocol.

Western blot analysis for muscle tissue and isolated mitochondria

Proteins were extracted from quadriceps femoris muscles or mitochondria isolated from forelimb and hindlimb muscles and suspended in SDS sample buffer; 125 mM Tris–HCl pH 6.8, 5% β-mercaptoethanol, 2% SDS and 10% glycerol. Extracted proteins were separated on acrylamide gels, and then transferred onto PVDF membranes (Millipore). Blocking solution of 5% skim milk was used. ImageQuant LAS 4000 Mini Biomolecular Imager (GE Healthcare) was used for evaluating bands.

Quantification of mtDNA by real-time PCR

Total DNA was isolated from triceps and quadriceps femoris and liver by proteinase K digestion and standard phenol–chloroform

extraction. Copy number of mtDNA (ND1) was quantified by real-time polymerase chain reaction (PCR) using SYBR Green PCR Kit (Qiagen) with *pcam1* as the control for the nuclear genome copy number. We used the following primers: ND1 forward primer, CCTATCACCCTTGCCATCAT; ND1 reverse primer, GAGGCTGTTGCTTGTGTGAC; *pcam1* DNA forward primer, ATGGAAAGCCTGCCATCATG; *pcam1* DNA reverse primer, TCCTTGTTGTTCAGCATCAC.

The amount of mtDNA relative to nuclear DNA was calculated using the following formula: mtDNA/nuclear DNA $= 2^{-(Ct_{mtDNA} - Ct_{nuclerDNA})}$ where Ct is the threshold cycle (22).

Morphometrical analysis of mitochondria

Cross-sectional EM image of extensor digitorum longus (EDL) muscle from *rmd* and littermates was analyzed by Image J software (23). Total areas of all mitochondria in 20 muscle fibers were calculated and compared with cross-sectional fiber areas. Total number of mitochondria per muscle fiber was counted.

Antibodies

Primary antibodies used were: mouse anti-4-hydroxy-2-nonenal (4-HNE) modified protein antibody (HNEJ-2,JalCA), rabbit anti-PINK1 antibody (BC100-494, Novus Biologicals), mouse anti-Parkin antibody (4211, Cell Signaling), rabbit anti-p62/SQSTM1 antibody (PWS860, Biomol), rabbit anti-LC3 antibody (NB100-2220, Novus Biologicals), mouse anti-poly-ubiquitin antibody (FK1, Biomol), rabbit anti-TOM20 antibody (FL-145, Santa Cruz), mouse anti-COX subunit 1 antibody (Invitrogen) and mouse anti-VDAC antibody (20B12, Santa Cruz). Second antibodies used were: horse radish peroxidase-labeled goat anti-mouse (Beckman Coulter) or rabbit antibodies (Cell Signaling), Alexa Fluor 488- and Alexa Fluor 568-labeled goat anti-mouse or rabbit antibodies (Invitrogen).

Statistical analysis

Data are presented as mean ± SD. Mean differences were compared with the analysis of *t*-test using R software version 2.11.0 (http://www.r-project.org/).

SUPPLEMENTARY MATERIAL

Supplementary Material is available at *HMG* online.

ACKNOWLEDGEMENTS

We thank Megumu Ogawa, Kanako Goto and Junko Takei for technical assistance.

FUNDING

This study was supported partly by the Research on Psychiatric and Neurological Diseases and Mental Health of Health and Labour Sciences Research Grants; partly by the Research on Intractable Diseases of Health and Labor Sciences Research Grants; partly by the Research Grant for Nervous and Mental Disorders (20B-12, 20B-13) from the Ministry of Health, Labour and Welfare; partly by an Intramural Research Grant (23-4, 23-5) for Neurological and Psychiatric Disorders from NCNP; partly by KAKENHI (20390250, 22791019); partly by Research on Publicly Essential Drugs and Medical Devices of Health and Labor Sciences Research Grants; partly by the Program for Promotion of Fundamental Studies in Health Sciences of the National Institute of Biomedical Innovation (NIBIO); and partly by the Grant from Japan Foundation for Neuroscience and Mental Health. G.A.C. and R.B.S. were supported in part by a National Institutes of Health Grant (AR054170 to G.A.C.).

REFERENCES

1. Mitsuhashi, S., Ohkuma, A., Talim, B., Karahashi, M., Koumura, T., Aoyama, C., Kurihara, M., Quinlivan, R., Sewry, C., Mitsuhashi, H. *et al.* (2011) A congenital muscular dystrophy with mitochondrial structural abnormalities caused by defective de novo phosphatidylcholine biosynthesis. *Am. J. Hum. Genet.*, **88**, 845–851.
2. Sher, R.B., Aoyama, C., Huebsch, K.A., Ji, S., Kerner, J., Yang, Y., Frankel, W.A., Hoppel, C.A., Wood, P.A., Vance, D.E. *et al.* (2006) A rostrocaudal muscular dystrophy caused by a defect in choline kinase beta, the first enzyme in phosphatidylcholine biosynthesis. *J. Biol. Chem.*, **281**, 4938–4948.
3. Saraste, M. (1999) Oxidative phosphorylation at the fin de siècle. *Science*, **283**, 1488–1493.
4. Spierings, D., McStay, G., Saleh, M., Bender, C., Chipuk, J., Maurer, U. and Green, D.R. (2005) Connected to death: the (unexpurgated) mitochondrial pathway of apoptosis. *Science*, **310**, 66–67.
5. Wakabayashi, T. (2002) Megamitochondria formation—physiology and pathology. *J. Cell Mol. Med.*, **6**, 497–538.
6. Benard, G., Bellance, N., James, D., Parrone, P., Fernandez, H. and Letellier, T. (2007) Mitochondrial bioenergetics and structural network organization. *J. Cell Sci.*, **120**, 838–848.
7. Yoon, Y.S., Yoon, D.S., Lim, I.K., Yoon, S.H., Chung, H.Y., Rojo, M., Malka, F., Jou, M.J., Martinou, J.C. and Yoon, G. (2006) Formation of elongated giant mitochondria in DFO-induced cellular senescence: involvement of enhanced fusion process through modulation of Fis1. *J. Cell Physiol.*, **209**, 468–480.
8. Karbowski, M., Kurono, C., Wozniak, M., Ostrowski, M., Teranishi, M., Nishizawa, Y., Usukura, J., Soji, T. and Wakabayashi, T. (1999) Free radical-induced megamitochondria formation and apoptosis. Free Radic. Biol. Med., **26**, 396–409.
9. Chen, H., Detmer, S.A., Ewald, A.J., Griffin, E.E., Fraser, S.E. and Chan, D.C. (2003) Mitofusins Mfn1 and Mfn2 coordinately regulate mitochondrial fusion and are essential for embryonic development. *J. Cell Biol.*, **160**, 189–200.
10. Chen, H., Chomyn, A. and Chan, D.C. (2005) Disruption of fusion results in mitochondrial heterogeneity and dysfunction. *J. Biol. Chem.*, **280**, 26185–26192.
11. Wu, G., Sher, R.B., Cox, G.A. and Vance, D.E. (2009) Understanding the muscular dystrophy caused by deletion of choline kinase beta in mice. *Biochim. Biophys. Acta*, **1791**, 347–356.
12. Daum, G. (1985) Lipids of mitochondria. *Biochim. Biophys. Acta*, **822**, 1–42.
13. Hayashi, Y.K., Matsuda, C., Ogawa, M., Goto, K., Tominaga, K., Mitsuhashi, S., Park, Y.E., Nonaka, I., Hino-Fukuyo, N., Haginoya, K. *et al.* (2009) Human PTRF mutations cause secondary deficiency of caveolins resulting in muscular dystrophy with generalized lipodystrophy. *J. Clin. Invest.*, **119**, 2623–2633.
14. Bligh, E.G. and Dyer, W.J. (1959) A rapid method of total lipid extraction and purification. *Can. J. Biochem. Physiol.*, **37**, 911–917.
15. Rouser, G., Fkeischer, S. and Yamamoto, A. (1970) Two dimensional then layer chromatographic separation of polar lipids and determination of phospholipids by phosphorus analysis of spots. *Lipids*, **5**, 494–496.
16. Mimaki, M., Hatakeyama, H., Ichiyama, T., Isumi, H., Furukawa, S., Akasaka, M., Kamei, A., Komaki, H., Nishino, I., Nonaka, I. *et al.* (2009)

Different effects of novel mtDNA G3242A and G3244A base changes adjacent to a common A3243G mutation in patients with mitochondrial disorders. *Mitochondrion*, **9**, 115–122.
17. Trounce, I.A., Kim, Y.L., Jun, A.S. and Wallace, D.C. (1996) Assessment of mitochondrial oxidative phosphorylation in patient muscle biopsies, lymphoblasts, and tranmitochondrial cell lines. *Methods enzymol.*, **264**, 484–509.
18. Vives-Bauza, C., Yang, L. and Manfredi, G. *Methods in Cell Biology. Mitochondria*, 2nd edn. Academic Press, London, UK, Vol. 80, Part 2, 7, 155–171.
19. Tang, P.H., Miles, M.V., Miles, L., Quinlan, J., Wong, B., Wenisch, A. and Bove, K. (2004) Measurement of reduced and oxidized coenzyme Q9 and coenzyme Q10 levels in mouse tissues by HPLC with coulometric detection. *Clin. Chim. Acta*, **341**, 173–184.
20. Wittig, I., Karas, M. and Schagger, H. (2007) High resolution clear native electrophoresis for in-gel functional assays and fluorescence studies of membrane protein complexes. *Mol. Cell Proteomics*, **6**, 1215–1225.
21. Armstrong, J.S. and Whiteman, M. *Methods in Cell Biology. Mitochondria*, 2nd edn. Academic Press, London, UK, Vol. 80, 18, 355–377.
22. Naini, A. and Shanske, S. *Methods in Cell Biology. Mitochondria*, 2nd edn. Academic Press, London, UK, Vol. 80, Part2, 22, 448–449.
23. Abramoff, M.D., Magelhaes, P.J. and Ram, S.J. (2004) Image processing with Image J. *Biophotonics Int.*, **11**, 36–42.
24. Zhang, M., Mileykovskaya, E. and Dowhan, W. (2002) Gluing the respiratory chain together. Cardiolipin is required for supercomplex formation in the inner mitochondrial membrane. *J. Biol. Chem.*, **277**, 43553–43556.
25. Geisler, S., Holmström, K.M., Skujat, D., Fiesel, F.C., Rothfuss, O.C., Kahle, P.J. and Springer, W. (2010) PINK1/Parkin-mediated mitophagy is dependent on VDAC1 and p62/SQSTM1. *Nat. Cell Biol.*, **12**, 119–131.
26. Narendra, D., Tanaka, A., Suen, D.F. and Youle, R.J. (2008) Parkin is recruited selectively to impaired mitochondria and promotes their autophagy. *J. Cell Biol.*, **183**, 795–803.
27. Lee, A.G. (2003) Lipid-protein interactions in biological membranes: a structural perspective. *Biochim. Biophys. Acta*, **1612**, 1–40.
28. Lange, C., Nett, J.H., Trumpower, B.L. and Hunte, C. (2001) Specific roles of protein-phospholipid interactions in the yeast cytochrome bc1 complex structure. *EMBO J.*, **20**, 6591–6600.
29. Hagopian, K., Weber, K.L., Hwee, D.T., Van Eenennaam, A.L., López-Lluch, G., Villalba, J.M., Burón, I., Navas, P., German, J.B., Watkins, S.M. *et al.* (2010) Complex I-associated hydrogen peroxide production is decreased and electron transport chain enzyme activities are altered in n-3 enriched fat-1 mice. *PLoS ONE*, **5**, e12696.
30. Balaban, R.S., Nemoto, S. and Finkel, T. (2005) Mitochondria, oxidants, and aging. *Cell*, **120**, 483–495.
31. St-Pierre, J., Buckingham, J.A., Roebuck, S.J. and Brand, M.D. (2002) Topology of superoxide production from different sites in the mitochondrial electron transport chain. *J. Biol. Chem.*, **277**, 44784–44790.
32. Osaki, Y., Nishino, I., Murakami, N., Matsubayashi, K., Tsuda, K., Yokoyama, Y.I., Morita, M., Onishi, S., Goto, Y.I. and Nonaka, I. (1998) Mitochondrial abnormalities in selenium-deficient myopathy. *Muscle Nerve*, **21**, 637–639.
33. Hill, K.E., Motley, A.K., Li, X., May, J.M. and Burk, R.F. (2001) Combined selenium and vitamin E deficiency causes fatal myopathy in guinea pigs. *J. Nutr.*, **131**, 1798–1802.
34. Rederstorff, M., Krol, A. and Lescure, A. (2006) Understanding the importance of selenium and selenoproteins in muscle function. *Cell Mol. Life Sci.*, **63**, 52–59.
35. Martensson, J. and Meister, A. (1989) Mitochondrial damage in muscle occurs after marked depletion of glutathione and is prevented by giving glutathione monoester. *Proc. Natl Acad. Sci. USA*, **86**, 471–475.
36. Choksi, K.B., Boylston, W.H., Rabek, J.P., Widger, W.R. and Papaconstantinou, J. (2004) Oxidatively damaged proteins of heart mitochondrial electron transport complexes. *Biochim. Biophys. Acta*, **1688**, 95–101.
37. Kim, I., Rodriguez-Enriquez, S. and Lemasters, J. (2007) Selective degradation of mitochondria by mitophagy. *Arch. Biochem. Biophys.*, **462**, 245–253.
38. Tatsuta, T. and Langer, T. (2008) Quality control of mitochondria: protection against neurodegeneration and ageing. *EMBO J.*, **27**, 306–314.
39. Ding, W.X., Ni, H.M., Li, M., Liao, Y., Chen, X., Stolz, D.B., Dorn, G.W. 2nd. and Yin, X.M. (2010) Nix is critical to two distinct phases of mitophagy, reactive oxygen species-mediated autophagy induction and Parkin-ubiquitin-p62-mediated mitochondrial priming. *J. Biol. Chem.*, **285**, 27879–27890.
40. Moraes, C.T., Shanske, S., Tritschler, H.J., Aprille, J.R., Andreetta, F., Bonilla, E., Schon, E.A. and DiMauro, S. (1991) mtDNA depletion with variable tissue expression: a novel genetic abnormality in mitochondrial diseases. Am. J. Hum. Genet., **48**, 492–501.
41. Kim, I. and Lemasters, J.J. (2011) Mitochondrial degradation by autophagy (mitophagy) in GFP-LC3 transgenic hepatocytes during nutrient deprivation. *Am. J. Physiol. Cell Physiol.*, **300**, C308–C317.

Autophagy 7:12, 1559–1561; December 2011; © 2011 Landes Bioscience

Phospholipid synthetic defect and mitophagy in muscle disease

Satomi Mitsuhashi and Ichizo Nishino*

Department of Neuromuscular Research; National Institute of Neuroscience; National Center of Neurology and Psychiatry; Tokyo, Japan

Mitophagy, selective autophagy of mitochondria, has been extensively demonstrated in cultured cell models but has never been described in skeletal muscle in the context of muscle disease. We recently reported the first example of human muscle disease where mitophagy plays a role in the peculiar muscle pathology. This disease is caused by loss-of-function mutations in the *CHKB* gene encoding choline kinase β. "Patients" and rostrocaudal muscular dystrophy (*rmd*) mice, spontaneous *Chkb* mutants, develop congenital muscular dystrophy with a peculiar mitochondrial abnormality—mitochondria are markedly enlarged at the periphery of muscle fibers and absent from the center. Choline kinase is the first enzymatic step in a biosynthetic pathway for phosphatidylcholine, the most abundant phospholipid in eukaryotes. Our discovery demonstrates that a phosphatydilcholine biosynthetic defect leads to mitochondrial dysfunction and increased mitophagy.

Keywords: choline kinase beta, phosphatidylcholine, mitochondria, mitophagy, congenital muscular dystrophy

Submitted: 08/02/11

Revised: 08/12/11

Accepted: 08/31/11

http://dx.doi.org/10.4161/auto.7.12.17925

*Correspondence to: Ichizo Nishino;
Email: nishino@ncnp.go.jp

Punctum to: Mitsuhashi S, Hatakeyama H, Karahashi M, Koumura T, Nonaka I, Hayashi YK, et al. . Muscle choline kinase beta defect causes mitochondrial dysfunction and increased mitophagy. Hum Mol Genet 2011; 20:3841–51; PMID:21750112; http://dx.doi.org/10.1093/hmg/ddr305

Congenital muscular dystrophy with mitochondrial structural abnormalities (CMDmt) (OMIM:602541) is an autosomal recessive disorder. "Patients" have various biallelic mutations—nonsense, missense or splice-site—in the *CHKB* gene. This is the only human disease caused by a phospholipid de novo synthetic enzyme defect. *rmd* mice have a 1.6-kb deletion in the *Chkb* gene, an ortholog of *CHKB*. Choline kinase activity in muscle is undetectable and the phosphatidylcholine level is decreased in muscles from both "patients" and *rmd* mice and also in isolated mitochondria from *rmd* mice (**Fig. 1**).

Interestingly, both CMDmt "patients" and *rmd* mice show distinct mitochondrial morphological abnormalities in muscle fibers: Mitochondria are nearly absent in the center, while they are enlarged at the periphery. This morphological change seems specific to this disease; we tested 15 "patients" with this distinct muscle pathology and identified mutations in *CHKB* gene in all of them. We hypothesize that altered phospholipid composition in muscle mitochondrial membrane may lead to mitochondrial structural and functional abnormalities.

In *rmd* mice, muscles are involved with the rostrocaudal gradient of severity; hindlimbs are more severely affected while forelimbs are relatively spared, and mitochondria are more sparse in hindlimbs. Isolated mitochondria from skeletal muscle of *rmd* mice show impaired respiratory chain enzyme activities, decreased ATP synthesis, and increased superoxide production. Not surprisingly, these mitochondrial bioenergetic dysfunctions are more severe in hindlimbs than in forelimbs, presumably reflecting the different degree of severity in muscle damage.

Mitochondrial bioenergetic abnormalities are also seen in mitochondrial myopathies; genetic diseases of the mitochondrial respiratory chain caused by a variety of defects in mtDNA or nuclear DNA. However, the muscle pathology of mitochondrial myopathies is different from that of CMDmt. In mitochondrial myopathies, mitochondria are commonly increased both in number and size in muscle fibers, showing a ragged red appearance upon modified Gomori trichrome staining. In contrast, in CMDmt, mitochondria are sparse in the center of muscle fibers, while they are enlarged at

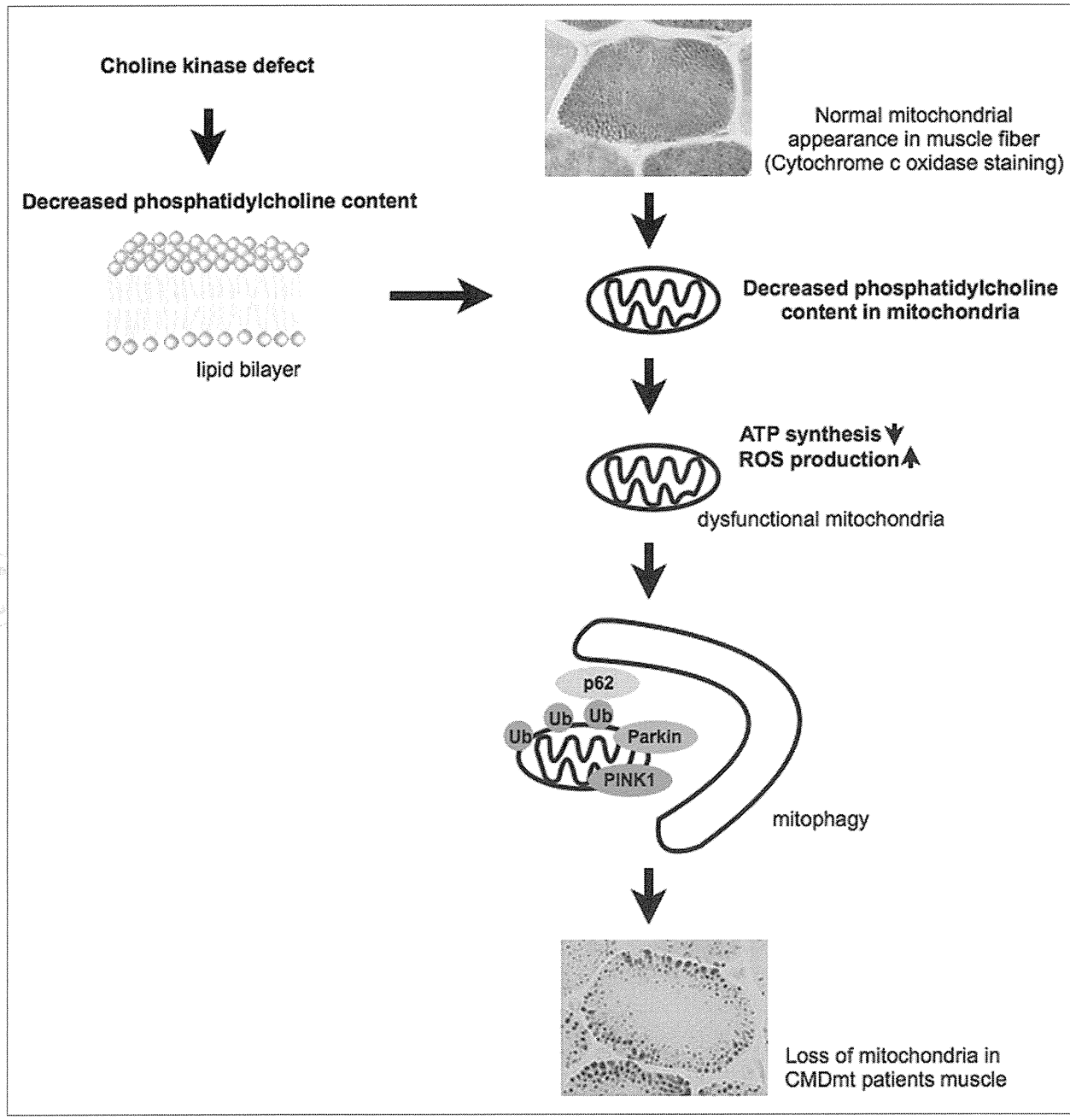

Figure 1. In normal muscle fiber, mitochondria distribute uniformly. Choline kinase defect causes a decreased phosphatidylcholine level in the mitochondrial membrane, leading to mitochondrial dysfunction. These mitochondria are eliminated by mitophagy, probably resulting in sparse mitochondria in muscle fiber.

the periphery. This mitochondrial decrease in number with concomitant increase in size can be confirmed by quantitative analysis in *rmd* mice. Mitochondrial DNA copy number is also decreased in *rmd* muscle in an age-dependent manner, most likely due to decreased mitochondrial number, because the pathological change of sparse mitochondria is also progressive with age.

In this disease, mitochondria are eliminated by mitophagy because (1) mitochondria are observed in autophagosomes by EM; (2) mitochondria are polyubiquitinated, and p62 and LC3 are recruited to mitochondria based on immunohistochemistry; and (3) PINK1 and Parkin in isolated mitochondria are increased based on western blotting, suggesting that they are recruited to mitochondria to promote mitophagy. Our data suggest that the decreased number of mitochondria is most likely due to increased mitochondrial clearance in skeletal muscle.

This discovery raises a number of important questions. Is it mitochondrial bioenergetic dysfunction that induces mitophagy in *rmd*? What will happen if mitophagy is blocked in *rmd* muscle? Does mitophagy have a protective role, or

promote muscle degeneration? In other words, is muscular dystrophy in *rmd* mice due to impaired mitochondria or excessive clearance of mitochondria?

Another important question is: How does membrane lipid compositional change affect mitochondrial function in vivo? Native PAGE analysis of *rmd* mitochondria shows that respiratory enzyme activity is decreased, but the respiratory chain protein complexes are properly formed. This finding supports the evidence that proper membrane lipid composition, and thereby lipid-protein interaction, is crucial for the activities of respiratory chain enzymes. Further study is necessary to elucidate the regulation mechanism of respiratory chain enzyme activities by membrane lipid.

CMDmt, due to the choline kinase β defect, should be a good model to investigate the regulation of mitochondrial number by mitophagy and lipid-protein interaction in mitochondrial membrane.

Acknowledgments

This study was supported partly by the Research on Psychiatric and Neurological Diseases and Mental Health of Health and Labour Sciences research grants; partly by Research on Intractable Diseases of Health and Labor Sciences research grants; partly by a Research Grant for Nervous and Mental Disorders (20B-12, 20B-13) from the Ministry of Health, Labour and Welfare; partly by an Intramural Research Grant (23-4, 23-5) for Neurological and Psychiatric Disorders from NCNP; partly by KAKENHI (20390250, 22791019); partly by Research on Publicly Essential Drugs and Medical Devices of Health and Labor Sciences research grants; partly by the Program for Promotion of Fundamental Studies in Health Sciences of the National Institute of Biomedical Innovation (NIBIO); and partly by a grant from the Japan Foundation for Neuroscience and Mental Health.

J Inherit Metab Dis
DOI 10.1007/s10545-011-9393-6

ORIGINAL ARTICLE

Effects of enzyme replacement therapy on five patients with advanced late-onset glycogen storage disease type II: a 2-year follow-up study

Yoshihiko Furusawa · Madoka Mori-Yoshimura · Toshiyuki Yamamoto · Chikako Sakamoto · Mizuki Wakita · Yoko Kobayashi · Yutaka Fukumoto · Yasushi Oya · Tokiko Fukuda · Hideo Sugie · Yukiko K. Hayashi · Ichizo Nishino · Ikuya Nonaka · Miho Murata

Received: 26 April 2011 / Revised: 4 September 2011 / Accepted: 8 September 2011

Abstract We examined the efficacy of 2-year enzyme replacement therapy (ERT) using recombinant human α-glucosidase (GAA; Myozyme®) in five long-term ventilator-dependent adults and aged patients with advanced, late-onset glycogen storage disease type II (GSDII, also known as Pompe disease). Although all patients had advanced respiratory failure and were ventilator-dependent for more than 6 years, four showed obvious improvements in muscle strength, pulmonary function, and activities of daily living after ERT. Improvement in each parameter was more prominent in the first year than in the second year. Values in the second year were still significantly better than those at study entry and indicate stabilization in the clinical status of all patients. These results suggest that ERT continues to be effective in the second year of treatment even in patients suffering from advanced late-onset GSDII disease with severe respiratory failure.

Introduction

Glycogen storage disease type II (GSDII), or Pompe disease, is an autosomal recessive lysosomal glycogen storage disease

Communicated by: Ed Wraith

Competing interests: None declared.

Electronic supplementary material The online version of this article (doi:10.1007/s10545-011-9393-6) contains supplementary material, which is available to authorized users.

Y. Furusawa · M. Mori-Yoshimura (✉) · T. Yamamoto · Y. Oya · M. Murata
Department of Neurology, National Center Hospital, National Center of Neurology and Psychiatry, 4-1-1 Ogawahigashi-cho, Kodaira, Tokyo 187-8551, Japan
e-mail: yoshimur@ncnp.go.jp

C. Sakamoto · M. Wakita · Y. Kobayashi
Department of Rehabilitation, National Center Hospital, National Center of Neurology and Psychiatry, 4-1-1 Ogawahigashi-cho, Kodaira, Tokyo 187-8551, Japan

Y. Fukumoto
Dental Branch, National Center Hospital, National Center of Neurology and Psychiatry, 4-1-1 Ogawahigashi-cho, Kodaira, Tokyo 187-8551, Japan

I. Nonaka
Department of Child Neurology, National Center Hospital, National Center of Neurology and Psychiatry, 4-1-1 Ogawahigashi-cho, Kodaira, Tokyo 187-8551, Japan

T. Fukuda · H. Sugie
Department of Pediatrics, Jichi Medical School, 3311-1, Yakushiji, Shimotsuke-city, Tochigi 329-0498, Japan

Y. K. Hayashi · I. Nishino
Department of Neuromuscular Research, National Institute of Neuroscience, National Center of Neurology and Psychiatry, 4-1-1 Ogawahigashi-cho, Kodaira, Tokyo 187-8502, Japan

Published online: 07 October 2011

resulting from a deficiency in α-glucosidase (GAA) activity (OMIM #232300). The different clinical phenotypes of GSDII include classic infantile-onset; non-classic infantile-onset; childhood, juvenile, and adult forms of GSDII; and late-onset GSDII. However, GSDII presents as a broad spectrum with varying degrees of severity and rates of progression. The classic infantile-onset form is characterized by hypertrophic cardiomyopathy and generalized muscle weakness, which appear in the first few months of life (Hirshhorn and Reuser 2001; Engel et al. 2004). Late-onset GSDII is characterized by progressive skeletal muscle weakness and loss of respiratory function.

Enzyme replacement therapy (ERT) using recombinant human GAA (rhGAA) derived from transfected Chinese hamster ovary cells resulted in marked improvement in the survival rate of 18 patients with infantile-onset GSDII (Kishnani et al. 2008). Nicolino and colleagues also reported that rhGAA reduced the risk of death and invasive ventilation by 79 and 58%, respectively, in infants and children with advanced Pompe disease (Nicolino et al. 2009). The use of ERT with Myozyme® (α-glucosidase) was approved by the U.S. Food and Drug Administration (FDA) in 2006 and by the Japan Ministry of Health, Labor and Welfare (MHLW) in 2007.

Previous studies confirmed the efficacy of ERT in late-onset GSDII patients with acute respiratory failure or relatively mild respiratory dysfunction (Winkel et al. 2004; Pascual-Pascual et al. 2006; Merk et al. 2007, 2009; Case et al. 2008; Yamamoto et al. 2008; Rossi et al. 2007; van Capelle et al. 2008; Strothotte et al. 2010; van der Ploeg et al. 2010). On the other hand, ERT efficacy in advanced patients seemed to be lower than that in milder patients (Orlikowski et al. 2011). It is not clear whether ERT is continuously effective in ventilator-dependent patients with advanced disease and long-term respiratory failure. Because ERT is relatively expensive, it is important to determine whether continuous administration is effective, or whether therapy is only effective for a short duration. In the present study, we evaluated the efficacy of ERT in five patients with advanced late-onset GSDII for 2 years and analyzed factors related to its efficacy.

Patients and methods

Patients

Patients with late-onset Pompe disease diagnosed based on both muscle biopsies and fibroblast/muscle residual GAA activity, and who had undergone ERT at the National Center Hospital (National Center of Neurology and Psychiatry), were included in this study. Written informed consent was obtained before enrollment. The study protocol was approved by the National Center Hospital Ethics Committee. Patients 4 and 5 have been reported previously (Sasaki et al. 1992; Yamazaki et al. 1992). Table 1 lists the characteristics of all five patients (two men and three women).

Genomic DNA was extracted from blood or muscle biopsy samples according to standard protocols. All exons and flanking intronic regions of GAA were amplified and sequenced using an automated 3100 DNA sequencer (Applied Biosystems, Foster, CA). Primer sequences are available upon request. All patients had previously reported mutations (Tsujino et al. 2000; Tsunoda et al. 1996; Lam et al. 2003; Pipo et al. 2003; Hermans et al. 2004). The average (SD) age at ERT initiation was 47 (13.6) years (range 32–66 years), and the average duration of disease was 26 (4.5) years (range 20–31 years). The average duration of mechanical ventilatory support before ERT was 8.0 (1.9) years (range 6–11 years). Patients 1, 2, 4, and 5 had been treated with noninvasive ventilation (NIV), and patient 3 had been treated with invasive ventilation. All patients were wheelchair-bound for a mean of 7.0 (5.1) years (range 2–14 years). Only patient 4 was able stand for a few minutes or walk a few steps with assistance. Others were completely wheelchair-bound.

Methods

ERT (Myozyme®) was administered at 20 mg/kg body weight biweekly at a dose of 1 mg/kg/h for the first 30 min, 3 mg/kg/h for the second 30 min, and then increased to 5 mg/kg/h, and finally 7 mg/kg/h every 30 min. Patients were carefully monitored for infusion-related reactions during and after ERT administration. Clinical condition was assessed every 6 months, including physical examination, manual muscle test (MMT), ECG, Holter ECG, ultrasound cardiography (UCG), and pulmonary function tests [% vital capacity (%VC), % force vital capacity (% FVC), forced expiratory volume in the first second (FEV1.0), peak expiratory flow rate (PEF), peak cough flow (PCF; Bach 2004)], and lean body mass (Discovery Bone Densitometer, Hologic, Bedford, MA). Muscle strength, including grip power (Dynamometer®, TTM, Japan, for patient 1; Grip Strength Dynamometer®, Takei, Japan, for patients 2–5) and pinch power (PinchTrack™, Jtech, Japan), was assessed every 2 weeks. The Barthel index and gross motor function measure manual (GMFM) were assessed every 6 months from the second year (Hosoda and Yanagisawa 2000; Kondo and Fukuda 2000). Occlusal force in the right and left first molar was measured using the Occlusal Force Meter GM10® (Nagano Keiki, Japan) every 6 months. In this test, which was repeated three times, patients were asked to bite on a block as hard as possible. All patients rested for more than 2 h before each muscle strength test. Normal values for grip power